analytical chemistry

Article

Cite This: *Anal. Chem.* 2019, 91, 14352−14358

pubs.acs.org/ac

1000-Fold Preconcentration of Per- and Polyfluorinated Alkyl Substances within 10 Minutes via Electrochemical Aerosol Formation

Yue Cao,[†,‡] Chuping Lee,[‡,§] Eric T. J. Davis,[‡] Weimeng Si,[†] Fagang Wang,[*,†] Sarah Trimpin,[*,‡] and Long Luo[*,‡]

[†]Shandong University of Technology, Zibo, Shandong 255000, China

[‡]Department of Chemistry, Wayne State University, Detroit, Michigan 48202, United States

[§]Department of Applied Chemistry, National Chiayi University, Chiayi 60004, Taiwan, Republic of China

Supporting Information

ABSTRACT: We present a simple and efficient method for preconcentrating per- and polyfluorinated alkyl substances (PFAS) in water. Our method was inspired by the sea-spray aerosol enrichment in nature. Gas bubbles in the ocean serve to scavenge surface active material, carrying it to the air-ocean interface, where the bubbles burst and form a sea-spray aerosol. These aerosol particles are enriched in surface-active organic compounds such as free fatty acids and anionic surfactants. In our method, we *in situ* generate H_2 microbubbles by electrochemical water reduction using a porous Ni foam electrode. These H_2 bubbles pick up PFAS as they rise through the water column that contains low concentration PFAS. When these bubbles reach the water surface, they burst and produce aerosol droplets that are enriched in PFAS. Using this method, we demonstrated ∼1000-fold preconcentration for ten common PFAS in the concentration range from 1 pM to 1 nM (or ∼0.5 ng/L to 500 ng/L) in 10 min. We also developed a diffusion-limited adsorption model that is in quantitative agreement with the experimental data. In addition, we demonstrated using this method to preconcentrate PFAS in tap water, indicating its potential use for quantitative analysis of PFAS in real-world water samples.

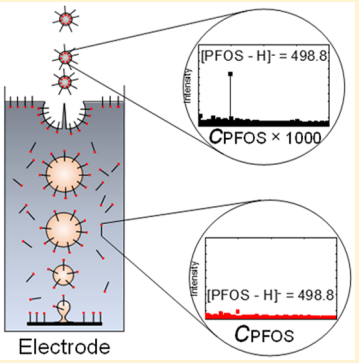

Per- and polyfluorinated alkyl substances (PFAS) are a group of anthropogenic compounds, some of which have been manufactured since the 1950s.[1] Due to their unique oleophobic and hydrophobic properties and high stability, PFAS are widely used in textile, upholstery, nonstick product manufacturing, aqueous film forming foams, and hydraulic fluids.[2,3] Widespread use and extreme resistance to degradation have resulted in the ubiquitous presence of these compounds in the environment. According to the previous studies,[4,5] the cumulative global emissions of PFAS are at least 46 000 tons with a large fraction released directly to the water systems. Recent results have shown PFAS can activate oxidative stress which is related to several diseases in humans, including atherosclerosis, heart attacks, chronic inflammatory diseases, central nervous system disorders, age-related disorders, and cancer.[6−9] Because of PFAS-related health concerns, the U.S. Environmental Protection Agency (EPA) published a health advisory for PFOS and PFOA—the two most common PFAS—in drinking water to be 70 ng/L individually or combined in 2016.[10] Following the EPA, some state governments have published stricter health advisories than the EPA standard. For example, Vermont's health advisory level for the sum of five PFAS should not exceed 20 ng/L in drinking water.[11] More recently, the state congress of Pennsylvania proposed that the State Environmental Quality Board shall adopt a maximum PFAS contaminant level as low as 5 ng/L.[12]

Detection of 5 ng/L PFAS in water, however, imposes an analytical challenge. The most commonly used analytical method for PFAS is EPA Method 537.[13] This method was established for determination of 18 different PFAS in drinking water using solid phase extraction and liquid chromatography/tandem mass spectrometry. The reported detection limit of this method varies among different laboratories but is typically a few ng/L which is just around the desired detection limit of 5 ng/L.[13,14] Besides, these detection limits are achieved by a 250-fold preconcentration using a multistep and time-consuming (up to several hours) solid-phase extraction before mass spectrometry detection.[13] Therefore, there is a critical need for a rapid and efficient preconcentration method for PFAS analysis.

Sea-spray aerosol enrichment is a well-known phenomenon in nature.[15−17] The ocean wind causes a near surface velocity gradient in the water column that results in wave breaking. The entrainment of air into the water column produces a plume of bubbles. These bubbles serve to scavenge surface-active

Received: June 17, 2019
Accepted: September 17, 2019
Published: September 17, 2019

DOI: 10.1021/acs.analchem.9b02758
Anal. Chem. 2019, 91, 14352−14358

material, carrying it to the air-ocean interface, where the bubbles burst and form a sea-spray aerosol.[18] These aerosol particles are enriched in surface-active organic materials such as free fatty acids and anionic surfactants.[16,17] Recently, Chen and co-workers[19−21] mimicked this phenomenon by generating gas bubbles in water using an air diffuser and collected the aerosol droplets formed by bubble bursting. They found the organic solutes in the aerosol were enriched by 6 to 12-fold for organic metabolites in urine (e.g., lipids and lipid-like molecules, phenylpropanoids and polyketides),[20] 20 to 1000-fold for rhodamine dyes,[21] and 10 to 100-fold for amino acids, protein, and DNA.[19]

Inspired by these previous studies, we developed a preconcentration method for PFAS that is based on electrochemical aerosol formation. Rather than using an external gas supply to generate bubbles, we *in situ* electrogenerated H_2 bubbles by water reduction (Scheme 1). The advantages of our design are 3-fold. First, electrogeneration of gas bubbles simplifies the design making miniaturization easy. Second, it allows additional modulation of the bubble formation by electrochemistry (e.g., controlling the bubble sizes and affecting the PFAS and electrode interactions by electrode potential). Third, it also improves the reproducibility of the aerosol-based enrichment by minimizing the initial momentum of gas bubbles, which helps to achieve a predictable low Reynolds number motion of bubbles,[22−24] and by reducing random bubble coalescence, which often occurs when using a porous frit to generate bubbles.[25] In this study, we demonstrate 1000-fold preconcentration of PFAS within 10 min using our method, taking advantage of the high surface activities of PFAS.[26]

Scheme 1. Preconcentration of PFAS via Electrochemical Aerosol Formation[a]

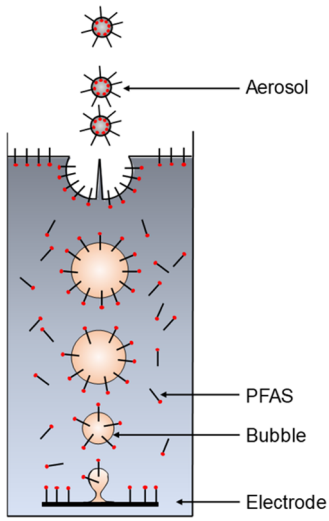

[a]Because of the high surface activity of PFAS, they will spontaneously adsorb and accumulate on the surface of gas bubbles. When the bubbles burst, only a thin layer of liquid surrounding the bubbles is ejected into the air resulting in a high concentration of PFAS in the aerosol droplets.

EXPERIMENTAL SECTION

Chemicals and Materials. Perfluorohexanoic acid (PFHxA, 97%), perfluoroheptanoic acid (PFHpA, 99%), perfluorooctanoic acid (PFOA, 95%), perfluorononanoic acid (PFNA, 97%), perfluorodecanoic acid (PFDA, 98%), perfluoroundecanoic acid (PFUnDA, 95%), perfluorododecanoic acid (PFDoDA, 95%), perfluorobutanesulfonic acid (PFBS, 98%), perfluorohexanesulfonic acid (PFHxS, 98%), perfluorooctanesulfonic acid (PFOS, 98%), sodium phosphate dibasic(99%), sodium phosphate monobasic (99%), methanol (99.9%), and nickel foam (mean aperture: 0.074 mm) were purchased from Sigma-Aldrich. Platinum electrodes were purchased from Aida Hengsheng (Tian Jin, China). Glass slides were purchased from Fisher Scientific. Deionized water (PURELAB, 18.2 MΩ cm, total organic carbon <3 ppb) was used in all the experimental processes.

Electrochemical Aerosol Enrichment. All the enrichment experiments were carried out in a home-built H-type two-compartment electrochemical cell (Figure S1). The cell was filled with ∼700 mL of 0.2 M phosphate buffer solution (pH = 7.0). A 1 cm × 1 cm Pt foil and a 1.5 cm × 1.5 cm Ni foam electrode were separately immersed in the two compartments and used as the anode and cathode, respectively. A constant voltage was applied between the two electrodes to electrolyze water. H_2 and O_2 bubbles were formed at the Ni electrode and Pt electrode, respectively. The aerosol produced by bubble bursting was collected using a slanted glass slide placed at ∼3 mm above the liquid surface (Figure S1). Twenty μL of the collected aerosol was transferred to a polypropylene microcentrifuge tube from the glass slide using a pipet.

Mass Spectrometry Analysis. Before analysis, the collected aerosols were diluted 20 times in 50:50 v:v H_2O/MeOH to ease sample handling and minimize chemical contamination of the mass spectrometer. Collected aerosols were analyzed operating a linear ion trap mass spectrometer (LTQ Velos, Thermo Fisher Scientific, San Jose, CA, United States)[27] with electrospray ionization. Mass spectra were acquired in the negative ion detection mode with a spray voltage of ±4.0 kV, respectively. The solvent flow was set at 0.010 mL/min, and data acquisitions time was 30 s. The transfer capillary was heated to 275 °C.

Bubble Size Analysis. Photographs of gas bubbles in the solution were taken using a Sony RX100 M4 (full manual mode, aperture f8, ISO 800, shutter speed 1/2000−1/1000 s) and analyzed using ImageJ software (NIH, Bethesda, MD) to obtain the bubble size distributions.

Finite Element Simulation. The finite element simulations were performed using COMSOL Multiphysics 5.3 (Comsol, Inc.) on a high-performance desktop PC. The simulation geometry, mesh, and boundary conditions are provided in the SI.

Tap Water Samples. Tap water was collected at the chemistry building of Wayne State University. No PFAS was found in the tap water sample. A mixture of PFAS was added to the tap water to prepare an artificial PFAS-contaminated tap water which contained 0.04 nM (16 ng/L) PFHxS, 0.02 nM (8 ng/L) PFOA, and 0.2 nM (100 ng/L) PFOS. The same procedure was used to preconcentrate PFAS as described above.

RESULTS AND DISCUSSION

Preconcentration of PFAS. We carried out this study using perfluorooctanesulfonic acid (PFOS) as the model analyte because it is one of the PFASs found most frequently and at the highest concentration in the environment and

DOI: 10.1021/acs.analchem.9b02758
Anal. Chem. 2019, 91, 14352−14358

humans.[28−31] We used a Ni foam with nominal aperture sizes of 0.074 mm as the cathode, a Pt foil as the anode, and 10^{-8} M (or 5 μg/L) PFOS in 0.2 M phosphate buffer (pH = 7.0) as the electrolyte. The Ni foam electrode was immersed at a depth of 25 cm. At a voltage of 70 V, the current level was ∼0.8 A, which corresponds to a volumetric flux of 5 mL of H_2 per minute. The radii of H_2 bubbles slightly increased from ∼0.05 mm to ∼0.08 mm with an average value of 0.07 mm as they rose to the water surface (Figure S2). The average bubble velocity was ∼1.2 cm/s. The aerosol droplets formed by bubble bursting were collected at a glass slide at ∼3 mm above the water surface (Figure S1). The collection rate of the aerosol droplets was estimated as ∼9 μL/min. After 5 min aerosol collection, millimeter-sized droplets were visible on the glass slide (Figure S1). To avoid chemical contamination of the mass spectrometer because of the high PFOS concentration in these droplets, we diluted 20 times using a 50/50 v/v H_2O and MeOH mixture before mass spectrometry analysis.

Figure 1a shows the mass spectra of diluted aerosol sample, two PFOS standards (5×10^{-7} M and 10^{-8} M both in 50/50 v/v H_2O and MeOH mixture), and the blank in the negative ion detection mode. These mass spectra were recorded and accumulated continuously throughout the acquisition of each sample for 30 s. The signal at mass-to-charge (m/z) = 498.8 corresponds to $[\text{PFOS} - \text{H}]^-$. We found good linearity between the signal intensity at m/z = 498.8 and the PFOS concentration in standard solutions ranging from 10^{-12} to 10^{-5} M (or 0.5 ng/L to 5 mg/L) with an r^2 value of 0.98 (Figures S3 and S4). Therefore, we directly used the signal intensity of $[\text{PFOS} - \text{H}]^-$ to quantify the PFOS in all collected aerosol samples. The diluted aerosol sample shows a similar concentration as the 5×10^{-7} M standard, indicating an enrichment factor of ∼1000-fold using our electrochemical aerosol formation method. The control experiments using 10^{-8} M standard and the blank show very low intensity at m/z = 498.8. We further tested other PFOS solutions with a concentration between 10^{-12} M and 10^{-8} M (or 0.5 ng/L to 5 μg/L) using our preconcentration method. At $C_{\text{PFOS,bulk}} < 10^{-9}$ M (or 500 ng/L), R is around 1000. At higher concentrations, R starts to decrease to ∼800. Overall, our preconcentration method has achieved an average R of 1000 ± 100 for PFOS. To test the reproducibility of our method, we carried out eight independent enrichment experiments following the same experimental protocol and measured the enrichment factors. We obtained a between-run coefficient of variation of 8% (Figure S5), indicating good producibility of our method.

Besides PFOS, we have also tested other 9 common PFAS including 7 perfluorinated carboxylic acids with carbon chain lengths from 6 to 12 (PFHxA, PFHpA, PFOA, PFNA, PFDA, PFUnDA, and PFDoDA) and 2 perfluorinated sulfonic acids (PFBS and PFHxS). We conducted the preconcentration experiments using a Ni foam electrode at an immersion depth of 25 cm and a voltage of 70 V for 10 min and then measured R using mass spectrometry. The information on the ion peaks used for quantitation is provided in Figures S3, S4, and S6 and Table S1. Figure 2 shows the R's for all 10 PFAS are close to ∼1000 at $C_{\text{PFAS, bulk}} = 10^{-10}$ M. The R slightly increases with the chain length of PFAS from ∼500 to 1300, which is probably caused by the increased surface activity. Most importantly, for each PFAS, the R-value varied by <10% at the concentration range of 10^{-12} to 10^{-9} M (Figure S7). The consistent enrichment performance of our method at a large concentration range makes it a promising technique for real-world applications.

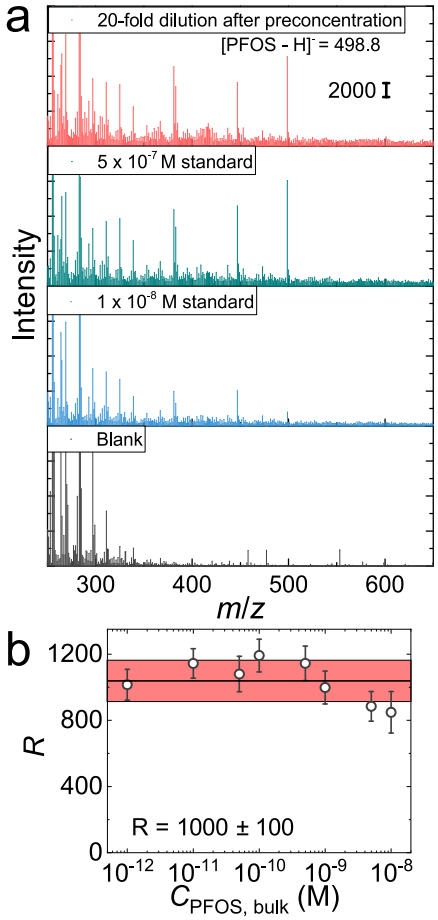

Figure 1. (a) Mass spectra of diluted aerosol sample, two PFOS standards (5×10^{-7} M and 10^{-8} M in a 50/50 v/v H_2O and MeOH mixture), and the blank in the negative ion detection mode. The aerosol sample was collected at 70 V for 10 min using 10^{-8} M PFOS solution as the electrolyte solution. The signals at m/z = 498.8 correspond to $[\text{PFOS} - \text{H}]^-$. (b) Enrichment factor, R, as a function of the PFOS concentration in the bulk solution ($C_{\text{PFOS,bulk}}$). R is defined as the ratio of PFOS concentrations in the aerosol ($C_{\text{PFOS,aerosol}}$) and its corresponding $C_{\text{PFOS,bulk}}$. The pink box shows the average and standard deviation of R's at all concentrations. The error bars are the standard deviations of three independent injections of the collected aerosol samples at each concentration.

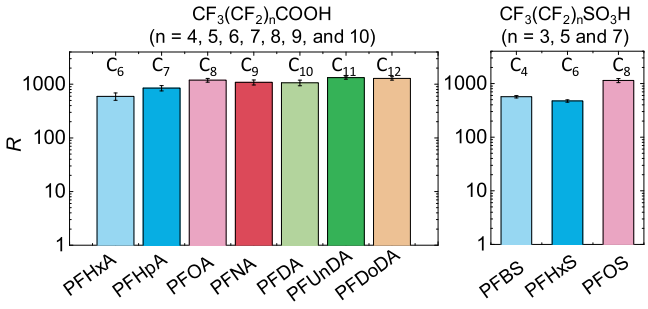

Figure 2. Enrichment factor, R, for 10 common PFAS including 7 perfluorinated carboxylic acids with carbon chain lengths from 6 to 12 (PFHxA, PFHpA, PFOA, PFNA, PFDA, PFUnDA, and PFDoDA) and 3 perfluorinated sulfonic acids (PFBS, PFHxS, and PFOS) at $C_{\text{PFAS,bulk}} = 10^{-10}$ M. Experimental conditions were identical to those in Figure 1.

DOI: 10.1021/acs.analchem.9b02758
Anal. Chem. 2019, 91, 14352−14358

Preconcentration Mechanism. To understand the preconcentration mechanism, we conducted a bubble path length (h) dependence study. We placed the Ni foam electrode at different depths of the electrolyte solution to control the interaction time between PFOS and H_2 bubbles. We did not observe any significant changes in current at different h (i = 0.74 ± 0.08 A) when a constant voltage of 70 V was applied. Figure 3 shows R vs h at different $C_{PFOS,bulk}$. At $C_{PFOS,bulk}$ = 10^{-11} M or 5 ng/L, there is a great linear relationship between R and h with a slope of 30 cm^{-1} and r^2 = 0.99. At $C_{PFOS,bulk}$ = 10^{-10} M and 10^{-9} M, we found the same linearity and slope. Until $C_{PFOS,bulk}$ was increased to 10^{-8} M, the R-value started deviating from the linearity and reached a plateau at h = 25 and 30 cm, suggesting the adsorption reached an equilibrium.

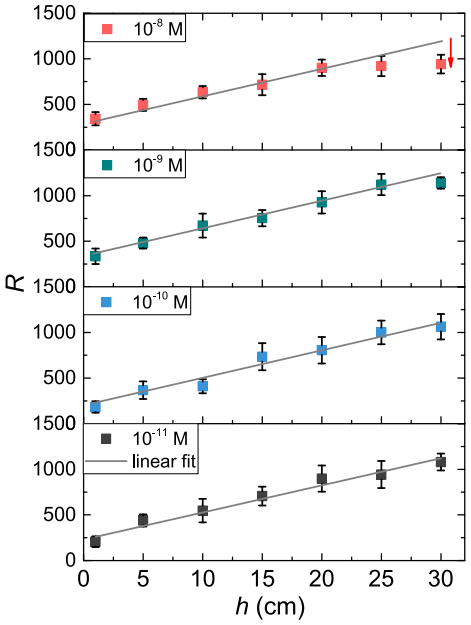

Figure 3. Plots of R vs h at different $C_{PFOS,bulk}$ from 10^{-11} to 10^{-8} M. At $C_{PFOS,bulk}$ = 10^{-11}, 10^{-10}, and 10^{-9} M, there is very similar linearity between R and h with a slope of 30 cm^{-1} and a y-intercept of ∼250. At $C_{PFOS,bulk}$ = 10^{-8} M and h > 20 cm, R starts deviating from such linearity.

To quantitatively understand the linearity in Figure 3, we first revisited a model previously developed by Chen and co-workers[21] for rhodamine dyes adsorption onto the surface of a rising spherical bubble. In their model, they assumed (1) the liquid near a bubble was renewed constantly due to bubble movement and (2) every surfactant that meets a rising bubble got adsorbed (the "total adsorption" model in Figure 4a). Based on these two assumptions, they expressed the total amount of surfactants adsorbed by a bubble (n) as the product of the solution volume that a bubble sweeps and the bulk concentration of surfactant (C_{bulk})

$$n = \pi r_{bubble}^2 h C_{bulk} \quad (1)$$

where r_{bubble} is the bubble radius. They then estimated the surfactant concentration in the aerosol, C_{aersol}, to be

$$C_{aerosol} \approx 150 C_{bulk} h / r_{bubble} \quad (2)$$

by relating the total volume of aerosol droplets produced by a single bubble to the bubble size.[32] Using eq 2 and our experimental conditions, we calculated the enrichment rate ($\partial R/\partial h$) to be 2.1 × 10^4 cm^{-1} which is 700 times our experimental result of 30 cm^{-1}.

To address this discrepancy, we propose a simple diffusion-limited adsorption model (Figure 4b). In our model, the liquid near a bubble is not renewed and moves at the same velocity as the rising bubble. Because PFOS has very high surface activity[33] and bubble surface is far from being saturated with PFOS during its lifetime, we assumed the bubble surface acted as a PFOS sink. Therefore, the adsorption of PFOS is limited by the diffusion of PFOS from the surrounding solution to the bubble surface. From electrochemical current and bubble velocity, we estimated there were approximately 10^6 H_2 bubbles in the bubble stream above the Ni foam electrode. The mean interbubble distance is, therefore, ∼360 μm. The "PFOS source" for a 70-μm-radius bubble is approximately a solution cube with a side length of 360 μm. Note that the size of a rising bubble was gradually increasing, so we used the average bubble radius of 70 μm for simplicity. Using these parameters, we simulated the diffusion of PFOS to bubble surface during the 20 s lifetime of a bubble using finite element simulation (see the SI). Figure 5 shows the simulated $C_{PFOS}/C_{PFOS,bulk}$ near a bubble as a function of time. The adsorbed PFOS, n_{PFOS}, linearly increases after 5 s. When $C_{PFOS,bulk}$ was set as 10^{-11} M, n_{PFOS} reaches 1.3 × 10^{-19} mol at t = 20 s accounting for ∼29% of the total available PFOS in the source. When a bubble bursts, it typically forms ∼5 aerosol droplets

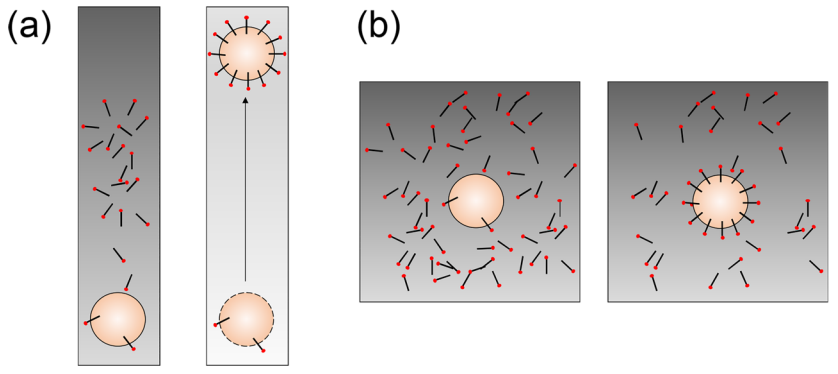

Figure 4. (a) The "total adsorption" model proposed by Chen and co-workers.[21] This model assumes that the liquid near a bubble was constantly renewed due to bubble movement, and every surfactant that meets a rising bubble was adsorbed. (b) Our diffusion-limited adsorption model. We assume the liquid near a bubble is not renewed during the rise of a bubble. The bubble surface acts as a PFAS sink. Diffusion of PFAS limits the adsorption rate.

DOI: 10.1021/acs.analchem.9b02758
Anal. Chem. 2019, 91, 14352−14358

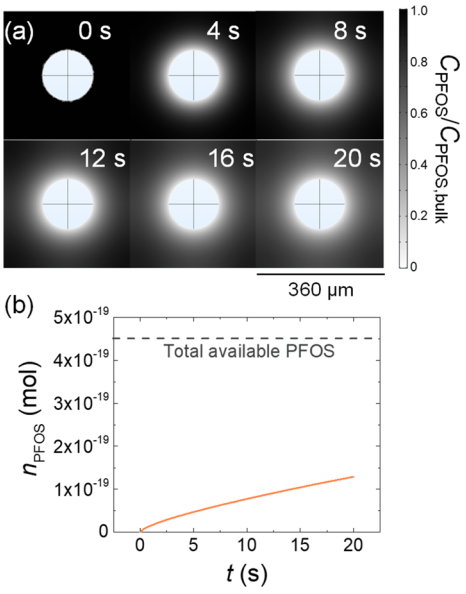

Figure 5. (a) Simulated $C_{PFOS}/C_{PFOS,bulk}$ near a 70-μm-radius gas bubble as a function of t. (b) The amount of PFOS adsorbed on the surface of a bubble (n_{PFOS}) as a function of t when $C_{PFOS,bulk} = 10^{-11}$ M.

with sizes of ~10% of the bubble size.[34] In other words, the ratio between the total volume of aerosol droplets and the corresponding bubble volume ($V_{aerosol}/V_{bubble}$) is 0.005. For a 70-μm-radius bubble, $V_{aerosol}$ should be $\sim 7.2 \times 10^{-12}$ L, giving a final $C_{PFOS,aerosol}$ of 1.8×10^{-8} M and an R of 1800. This simulated R using our diffusion-limited model is close to the experimental value of 1140 ± 90 at $C_{PFOS,bulk} = 10^{-11}$ M in Figure 1b.

Now, we move on to derive the analytical expression of enrichment rate ($\partial R/\partial h$). The simulation result in Figure 5b shows that the diffusion of PFOS reaches a quasi-steady state after ~5 s. This is caused by the spherical diffusion field of PFOS near a gas bubble. The growth of the PFOS depletion region fails to significantly affect the concentration gradients at the surface because the diffusion field is able to draw material from a continually larger area at its outer limit.[35] The solution of the diffusion equation in a spherical diffusion field at steady state is given by[35]

$$\frac{\partial n_{PFOS}}{\partial t} = \frac{A_{bubble} D_{PFOS} C_{PFOS,bulk}}{r_{bubble}} \quad (3)$$

where D_{PFOS} is the diffusion coefficient of PFOS in water, and A_{bubble} is the surface area of a bubble. We obtain the expression of $C_{PFOS,aerosol}$ after approximating t as the ratio of h to the average bubble velocity (v_{bubble}) and using the empirical $V_{aerosol}/V_{bubble}$ ratio of 0.005 described above.[34]

$$C_{PFOS,aerosol} = \frac{200 A_{bubble} D_{PFOS} C_{PFOS,bulk} h}{r_{bubble} v_{bubble} V_{bubble}} \quad (4)$$

which can be then rearranged to yield

$$\frac{\partial R}{\partial h} = \frac{200 A_{bubble} D_{PFOS}}{r_{bubble} v_{bubble} V_{bubble}} \quad (5)$$

As v_{bubble} can be estimated by Stokes' law,[36] eq 5 is simplified as

$$\frac{\partial R}{\partial h} = 2.4 \times 10^{-4} [\mathrm{m^2 \cdot s}] \frac{D_{PFOS}}{r_{bubble}^4} \quad (6)$$

Using $D_{PFOS} = 0.4 \times 10^{-9}$ m^2/s[37] and $r_{bubble} = 70$ μm, eq 6 predicts an enrichment rate of 40 cm^{-1} which is close to the experimental value of 30 cm^{-1} in Figure 3. The great agreement between our prediction and experimental data again confirms our diffusion-limited adsorption model. Please note that this model may underestimate the enrichment rate for bubbles generated by pushing high-pressure gas through a microporous membrane where substantial convective mass transfer, as well as the turbulent flow, can take place.

Next, we discuss the enrichment plateau at $C_{PFOS,bulk} = 10^{-8}$ M and $h > 20$ cm (Figure 3). This plateau indicates the PFOS in the solution and on the bubble surface have reached an equilibrium. To further confirm this, we estimated the air–water interface adsorption coefficient, K, by

$$K = \frac{\Gamma_{PFOS}}{C_{PFOS,bulk}} \approx R \frac{0.005 V_{bubble}}{A_{bubble}} \quad (7)$$

where Γ_{PFOS} is the surface excess concentration of PFOS at equilibrium. We obtained a K value of 0.011 cm for a 70-μm-radius gas bubble. This value is in good agreement with the literature value of 0.014 cm,[38,39] confirming the enrichment plateau is caused by the adsorption equilibrium of PFOS.

Finally, another interesting finding is the large intercepts of the R vs h plots in Figure 3. At a bubble path close to zero, the enrichment factor is still as high as 250, accounting for ~25% of the total enrichment. In comparison, Chen and co-workers only observed an enrichment factor of ~30 at zero-bubble path using their aerosol enrichment setup.[21] This difference may be caused by electrode-PFOS interactions, which increase local PFOS concentration near the electrode surface.

Modulating the Preconcentration by Electrochemistry. According to eq 6, the enrichment rate ($\partial R/\partial h$) is inversely proportional to the fourth order of bubble radius (r_{bubble}^4). To test it, we tuned bubble size by applying different voltages. Figure S2 shows the average r_{bubble} increases slowly with the applied voltage from 0.045 mm at 30 V to 0.064 mm at 80 V. The corresponding current increased from 0.31 to 0.98 A, the enrichment factor, R, decreased from 2600 to 1200, and the enrichment rate, $\partial R/\partial h$, decreased from ~100 to ~30 cm^{-1} (Figure 6). After fitting the plot of $\partial R/\partial h$ vs r_{bubble} in the form of eq 6, we obtained a D_{PFOS} value of 0.22×10^{-9} which is in a reasonable agreement with the literature value of 0.4×10^{-9} m^2/s.[37] The good agreement confirms our model and also

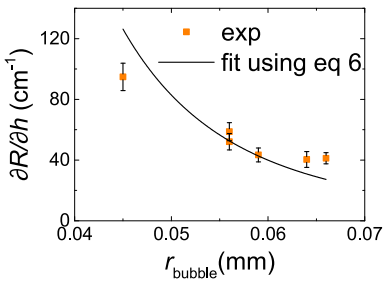

Figure 6. Enrichment rate, $\partial R/\partial h$, as a function of r_{bubble} and the fit of experimental data in the form of eq 6. The average radii of bubbles, r_{bubble}, was tuned by applying different voltages from 30 to 80 V. Other experimental conditions: $h = 25$ cm and $C_{PFOS,bulk} = 10^{-10}$ M.

DOI: 10.1021/acs.analchem.9b02758
Anal. Chem. 2019, 91, 14352−14358

indicates that the enrichment process can be readily modulated by electrochemistry.

Preconcentration of PFAS in Tap Water. To test the performance of this preconcentration method for real-world samples, we collected tap water at the chemistry building of Wayne State University and spiked the tap water with a mixture of PFHxS, PFOA, and PFOS. The PFAS concentrations in the unspiked tap water are below the detection limit of mass spectrometer (Figure S9). Even after preconcentration, no PFAS signal was observed (Figure 7a). The spiked tap water contains 0.04 nM (16 ng/L) PFHxS, 0.02 nM (8 ng/L) PFOA, and 0.2 nM (100 ng/L) PFOS. This PFAS pattern is the same as that found in Robinson Elementary School's drinking water on October 29, 2018, in Grand Haven, MI.[40] After preconcentration, the mass spectrum shows the signals of PFHxS, PFOA, and PFOS (Figure 7a). The C_{PFAS} in the aerosol sample is then calculated from these mass spectrometry signals, yielding an enrichment factor, $R_{measured}$, of 490 ± 60, 870 ± 90, and 910 ± 70 for PFHxS, PFOA, and PFOS, respectively. These $R_{measured}$ values are in good agreement (~10% difference) with the $R_{expected}$ values determined using the standard solutions (Figure 1b and Figure S7). The consistent enrichment performance indicates the potential analytical utility of our preconcentration method in analyzing ultralow concentration PFAS in real-world water samples.

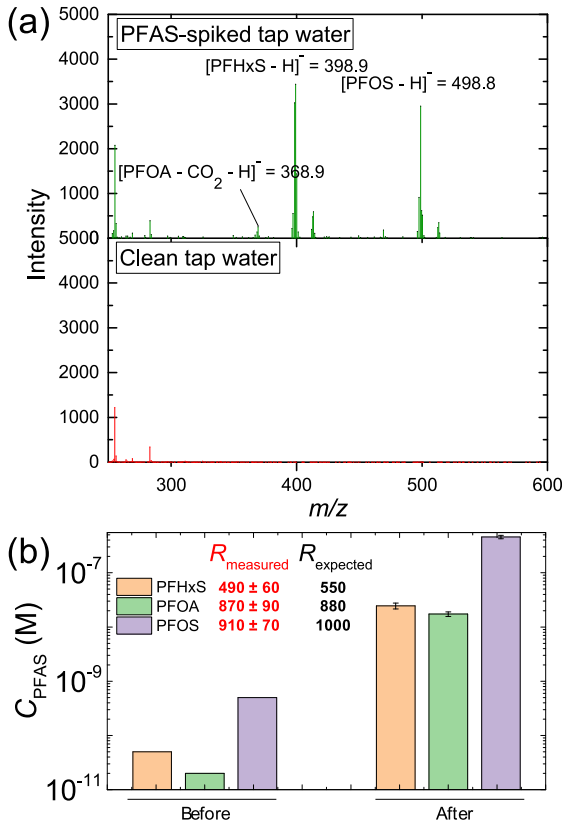

Figure 7. (a) Mass spectra of two 20-fold diluted aerosol samples, which were collected at 70 V for 10 min using PFAS-spiked tap water (top) and clean tap water without spiking (bottom) as the electrolyte solution, respectively. The signals at m/z = 368.9, 398.9, and 498.8 correspond to $[PFOA\text{-}CO_2{-}H]^-$, $[PFHxS - H]^-$, and $[PFOS - H]^-$, respectively. The tap water was collected at the chemistry building of Wayne State University. After spiking, the tap water contained a mixture of 0.04 nM (16 ng/L) PFHxS, 0.02 nM (8 ng/L) PFOA, and 0.2 nM (100 ng/L) PFOS. (b) PFAS concentrations before and after preconcentration. The measured preconcentration factor, $R_{measured}$, vs the expected preconcentration factor, $R_{expected}$, for each PFAS compound spiked in the tap water. The $R_{expected}$ values are the average R values for each PFAS compound at concentrations from 10^{-12} to 10^{-9} M.

CONCLUSIONS

In conclusion, we have presented a simple and efficient method for preconcentrating PFAS in water via electrochemical aerosol formation. We have demonstrated 1000-fold enrichment of 10 common PFAS within 10 min. For each PFAS, the enrichment factor shows less than 10% variation at the concentration range of 10^{-12} to 10^{-9} M. We have built a diffusion-limited adsorption theory for this electrochemical aerosol enrichment method and validated it. We have also demonstrated using this method to preconcentrate PFAS in tap water, indicating it can be useful for addressing the current challenges in analyzing ultralow concentration PFAS in water.

ASSOCIATED CONTENT

Supporting Information

The Supporting Information is available free of charge on the ACS Publications website at DOI: 10.1021/acs.analchem.9b02758.

Photographs of experimental setup; plots of r_{bubble} vs h at various voltages from 30 to 80 V; mass spectra of PFAS standards; calibration curves for PFAS; enrichment factor for 9 common PFAS at different concentrations; reproducibility test results; geometry, mesh, and parameters of our finite element simulation model; mass spectrum of unspiked tap water sample; mass-to-charge (m/z) signals used for quantifying PFAS (PDF)

AUTHOR INFORMATION

Corresponding Authors

*E-mail: long.luo@wayne.edu.
*E-mail: strimpin@chem.wayne.edu.
*E-mail: a_gang@sdut.edu.cn.

ORCID

Sarah Trimpin: 0000-0002-3720-2269
Long Luo: 0000-0001-5771-6892

Notes

Any opinions, findings, and conclusions or recommendations expressed in this material are those of the authors and do not necessarily reflect the views of the National Science Foundation.
The authors declare no competing financial interest.

ACKNOWLEDGMENTS

This work was supported by start-up funds, Ebbing Faculty Development Award, and University Research Grant from Wayne State University to L.L. The authors are grateful for funding and support from NSF CHE-1411376 to S.T. We also thank Xuecheng Yu for his help with the bubble sizing.

REFERENCES

(1) Mejia-Avendaño, S.; Munoz, G.; Sauve', S. b.; Liu, J. *Anal. Chem.* **2017**, *89*, 2539−2546.
(2) Seow, J. *Fire Fighting Foams with Perfluorochemicals-Environmental Review*; Hemming Information Services: 2013.

DOI: 10.1021/acs.analchem.9b02758
Anal. Chem. 2019, 91, 14352−14358

(3) Fiedler, S.; Pfister, G.; Schramm, K.-W. *Toxicol. Environ. Chem.* **2010**, *92*, 1801−1811.
(4) Wang, Z.; Cousins, I. T.; Scheringer, M.; Buck, R. C.; Hungerbühler, K. *Environ. Int.* **2014**, *70*, 62−75.
(5) Paul, A. G.; Jones, K. C.; Sweetman, A. J. *Environ. Sci. Technol.* **2009**, *43*, 386−392.
(6) Berthiaume, J.; Wallace, K. B. *Toxicol. Lett.* **2002**, *129*, 23−32.
(7) Hu, W.; Jones, P. D.; Upham, B. L.; Trosko, J. E.; Lau, C.; Giesy, J. P. *Toxicol. Sci.* **2002**, *68*, 429−436.
(8) Wielsøe, M.; Long, M.; Ghisari, M.; Bonefeld-Jørgensen, E. C. *Chemosphere* **2015**, *129*, 239−245.
(9) Richardson, S. D.; Ternes, T. A. *Anal. Chem.* **2018**, *90*, 398−428.
(10) U. S. Environmental Protection Agency. Drinking Water Health Advisories for PFOA and PFOS. https://www.epa.gov/ground-water-and-drinking-water/drinking-water-health-advisories-pfoa-and-pfos (accessed January 18, 2019).
(11) State of Vermont, Department of Health. Commissioner's Office, Drinking Water Health Advisory for Five PFAS (Per- and Polyfluorinated Alkyl Substances). http://www.healthvermont.gov/sites/default/files/documents/pdf/ENV_DW_PFAS_HealthAdvisory.pdf (accessed June 5, 2019).
(12) The General Assembly of Pennsylvania, House Bill No 705, Session of 2017. https://www.legis.state.pa.us/CFDOCS/Legis/PN/Public/btCheck.cfm?txtType=PDF&sessYr=2017&sessInd=0&billBody=H&billTyp=B&billNbr=0705&pn=0755 (accessed June 5, 2019).
(13) Shoemaker, J.; Grimmett, P.; Boutin, B. Method 537. Determination of Selected Perfluorinated Alkyl Acids in Drinking Water by Solid Phase Extraction and Liquid Chromatography/Tandem Mass Spectrometry (LC/MS/MS). https://www.epa.gov/water-research/epa-drinking-water-research-methods (accessed July 12, 2019).
(14) Prakash, W. L. B. *Comparison of ASTM D7979 PFAS Compounds by the ASTM Method versus Solid Phase Extraction*; Eurofins Eaton Analytical: 2018.
(15) Aller, J. Y.; Kuznetsova, M. R.; Jahns, C. J.; Kemp, P. F. *J. Aerosol Sci.* **2005**, *36*, 801−812.
(16) McMurdo, C. J.; Ellis, D. A.; Webster, E.; Butler, J.; Christensen, R. D.; Reid, L. K. *Environ. Sci. Technol.* **2008**, *42*, 3969−3974.
(17) Bertram, T. H.; Cochran, R. E.; Grassian, V. H.; Stone, E. A. *Chem. Soc. Rev.* **2018**, *47*, 2374−2400.
(18) Wilson, T. W.; Ladino, L. A.; Alpert, P. A.; Breckels, M. N.; Brooks, I. M.; Browse, J.; Burrows, S. M.; Carslaw, K. S.; Huffman, J. A.; Judd, C.; et al. *Nature* **2015**, *525*, 234.
(19) Chingin, K.; Cai, Y.; Liang, J.; Chen, H. *Anal. Chem.* **2016**, *88*, 5033−5036.
(20) Chingin, K.; Cai, Y.; Chagovets, V.; Kononikhin, A.; Starodubtseva, N.; Frankevich, V.; Chen, H. *Metabolomics* **2016**, *12*, 171.
(21) Chingin, K.; Yan, R.; Zhong, D.; Chen, H. *ACS Omega* **2018**, *3*, 8709−8717.
(22) Magnaudet, J.; Eames, I. *Annu. Rev. Fluid Mech.* **2000**, *32*, 659−708.
(23) Taqieddin, A.; Nazari, R.; Rajic, L.; Alshawabkeh, A. *J. Electrochem. Soc.* **2017**, *164*, E448−E459.
(24) Taqieddin, A.; Allshouse, M. R.; Alshawabkeh, A. N. *J. Electrochem. Soc.* **2018**, *165*, E694−E711.
(25) Wang, X.; Deane, G. B.; Moore, K. A.; Ryder, O. S.; Stokes, M. D.; Beall, C. M.; Collins, D. B.; Santander, M. V.; Burrows, S. M.; Sultana, C. M. *Proc. Natl. Acad. Sci. U. S. A.* **2017**, *114*, 6978−6983.
(26) Shinoda, K.; Hato, M.; Hayashi, T. *J. Phys. Chem.* **1972**, *76*, 909−914.
(27) El-Baba, T. J.; Lutomski, C. A.; Wang, B.; Trimpin, S. *Rapid Commun. Mass Spectrom.* **2014**, *28*, 1175−1184.
(28) Huset, C. A.; Chiaia, A. C.; Barofsky, D. F.; Jonkers, N.; Kohler, H.-P. E.; Ort, C.; Giger, W.; Field, J. A. *Environ. Sci. Technol.* **2008**, *42*, 6369−6377.
(29) Loos, R.; Gawlik, B. M.; Locoro, G.; Rimaviciute, E.; Contini, S.; Bidoglio, G. *Environ. Pollut.* **2009**, *157*, 561−568.
(30) Murakami, M.; Imamura, E.; Shinohara, H.; Kiri, K.; Muramatsu, Y.; Harada, A.; Takada, H. *Environ. Sci. Technol.* **2008**, *42*, 6566−6572.
(31) Kärrman, A.; Ericson, I.; van Bavel, B.; Darnerud, P. O.; Aune, M.; Glynn, A.; Lignell, S.; Lindström, G. *Environ. Health Perspect.* **2007**, *115*, 226−230.
(32) Brasz, C. F.; Bartlett, C. T.; Walls, P. L.; Flynn, E. G.; Yu, Y. E.; Bird, J. C. *Phys. Rev. Fluids* **2018**, *3*, 074001.
(33) Schultz, M. M.; Barofsky, D. F.; Field, J. A. *Environ. Eng. Sci.* **2003**, *20*, 487−501.
(34) Kientzler, C. F.; Arons, A. B.; Blanchard, D. C.; Woodcock, A. H. *Tellus* **1954**, *6*, 1−7.
(35) Bard, A. J.; Faulkner, L. R. *Electrochemical Methods: Fundamentals and Applications*; Wiley: New York, 1980.
(36) Batchelor, C. K.; Batchelor, G. *An Introduction to Fluid Dynamics*; Cambridge University Press: 1967.
(37) Pereira, L. A. M.; Martins, L. F. G.; Ascenso, J. R.; Morgado, P.; Ramalho, J. P. P.; Filipe, E. J. M. *J. Chem. Eng. Data* **2014**, *59*, 3151−3159.
(38) Chen, W. *Adsorption and Retardation of PFAS in Soils*; University of Arizona: 2018.
(39) Lyu, Y.; Brusseau, M. L.; Chen, W.; Yan, N.; Fu, X.; Lin, X. *Environ. Sci. Technol.* **2018**, *52*, 7745−7753.
(40) The State of Michigan, Robinson Elementary School Drinking Water Response. https://www.michigan.gov/pfasresponse/0,9038,7-365-86510_88061_88064-483785--,00.html (accessed Sep 7, 2019).

DOI: 10.1021/acs.analchem.9b02758
Anal. Chem. 2019, 91, 14352−14358